# Ozone Initiates Human-Derived Emission of Nanocluster Aerosols

(article starts on next page)

# Ozone Initiates Human-Derived Emission of Nanocluster Aerosols

Shen Yang, Dusan Licina,* Charles J. Weschler, Nijing Wang, Nora Zannoni, Mengze Li, Joonas Vanhanen, Sarka Langer, Pawel Wargocki, Jonathan Williams, and Gabriel Bekö*

ACCESS | Metrics & More | Article Recommendations | Supporting Information

**ABSTRACT:** Nanocluster aerosols (NCAs, particles <3 nm) are important players in driving climate feedbacks and processes that impact human health. This study reports, for the first time, NCA formation when gas-phase ozone reacts with human surfaces. In an occupied climate-controlled chamber, we detected NCA only when ozone was present. NCA emissions were dependent on clothing coverage, occupant age, air temperature, and humidity. Ozone-initiated chemistry with human skin lipids (particularly their primary surface reaction products) is the key mechanism driving NCA emissions, as evidenced by positive correlations with squalene in human skin wipe samples and known gaseous products from ozonolysis of skin lipids. Oxidation by OH radicals, autoxidation reactions, and human-emitted $NH_3$ may also play a role in NCA formation. Such chemical processes are anticipated to generate aerosols of the smallest size (1.18−1.55 nm), whereas larger clusters result from subsequent growth of the smaller aerosols. This study shows that whenever we encounter ozone indoors, where we spend most of our lives, NCAs will be produced in the air around us.

**KEYWORDS:** *ozone chemistry, indoor air, human skin lipids, particle formation, molecular clusters*
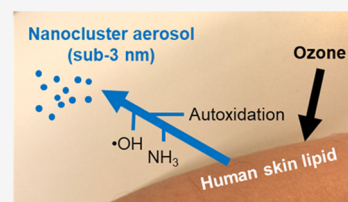
## INTRODUCTION

Airborne nanoparticles of sub-3 nm size are termed nanocluster aerosol (NCA) particles. By number, NCA particles constitute a considerable fraction of urban aerosols as they originate directly from traffic emissions[1] and via atmospheric processes,[2] with number concentrations ranging from $10^2$ to $10^5$ $cm^{-3}$.[3] Previous studies have shown that NCAs are precursors of new nanoparticle formation,[4] which is a key phenomenon associated with the growth of atmospheric aerosol particles into cloud condensation nuclei and hence climate feedbacks.[5]

Owing to recent advancements in fast-response and high-time-resolution NCA measurement technologies,[6] recent indoor studies have started to reveal the importance of NCA characterization in this relatively understudied environment. Results from a field campaign in a test house with periodic occupancy showed that NCAs could dominate total particle number, particularly during cooking and dining ($10^5$ to $10^6$ $cm^{-3}$).[7] It has been shown previously that considerable numbers of NCAs can be generated from cooking,[8] burning candles,[9] 3D printing,[10] and thermal desorption of semivolatile organic compounds (SVOCs).[11] Although the specific health impacts of NCAs remain unknown, exposure to elevated concentrations of nanoparticles (<100 nm) has been linked to adverse health outcomes, due to their deep penetration into the human lung and even neuronal transport to the brain.[12]

The impact of ozone on NCA formation from reactive gas-phase pollutants is well-documented outdoors.[13] It can be hypothesized that ozone-initiated NCA generation indoors occurs at an even greater extent, owing to the large surface-to-volume ratios promoting surface chemistry[14] and the presence of diverse and abundant VOCs[15] and other precursors available for ozone chemistry.[16]

Humans and their clothing play an important role in indoor ozone chemistry. Skin lipids contain squalene and unsaturated fatty acids, which rapidly react with ambient ozone.[17] These reactions are a potent source of indoor carbonyls, dicarbonyls, and hydroxycarbonyls.[18−21] Reaction of ozone with human skin or previously worn clothing also generates ultrafine particles in the 10−100 nm diameter range.[22,23] These ultrafine particles presumably originate from the growth of NCA, as has been observed in outdoor air,[24,25] although this has not yet been demonstrated.

This study reports NCA formation from ozone−human chemistry and the associated driving parameters. Within the framework of the Indoor Chemical Human Emissions and Reactivity (ICHEAR) project,[26] we measured the emission of 1.18−4 nm aerosol particles from human volunteers in the absence and presence of ozone within a climate-controlled chamber. We investigated the effects of the extent of clothing (covered body surface area), air temperature and humidity, and the age of the human subjects. Together with highly sensitive VOC and OH reactivity measurements, we probed
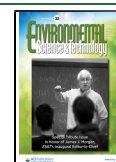
the underlying mechanisms and principal drivers responsible for the observed NCA formation.

## METHODS

**Climate Chamber.** A detailed description and experimental methodology are given in Bekö et al.[26] Briefly, measurements were made in a 22.5 m$^3$ stainless-steel climate-controlled chamber (Figure S1).[26,27] The chamber was ventilated with 100% outdoor air at an air change rate of 3.2 ± 0.1 h$^{-1}$. A combination of newly installed F7 fiber filters and high-efficiency activated carbon molecular filters ensured an NCA- and ozone-free background in the unoccupied chamber (<1 NCA/cm$^3$ and <1 ppb, respectively). The air was supplied through the perforated floor and exhausted via an outlet in the ceiling, where NCA concentrations were measured. During conditions with ozone present, ozone was generated in the supply air duct using a Jelight 600 UV generator (Jelight Co. Inc., USA). The chamber was furnished with a table and four wire mesh metal chairs. Additionally, two pedestal fans facing the chamber walls ensured air mixing. To minimize reactive surfaces other than human volunteers, the chamber and furniture surfaces were thoroughly cleaned prior to the experimental campaign and at regular intervals during the campaign.

**Experimental Procedure.** Five groups of four human volunteers were recruited: three young-adult groups (A1−A3; average age 25.1 years, range 19−30), one teenager group (T4; average age 13.8 years, range 13−15), and one senior group (S5; average age 70.5 years, range 68−72). NCA emissions were investigated for groups A1, A2, T4, and S5. Groups A2, T4, and S5 consisted of two males and two females, while group A1 included three males and one female.

The volunteers were asked to take a shower in the evening prior to experiments using provided perfume- and odorant-free liquid soap and shampoo. They were asked not to apply any personal-care products. Prior to entering the chamber the following morning, the volunteers were asked to change into a set of clothes provided by the researchers. The clothing was washed with perfume- and odorant-free laundry detergent once directly after purchase, tumble-dried, and sealed in individual zip-lock bags. In the chamber, the volunteers sat around the table and were allowed to use their smartphones or provided computer tablets. They were not allowed to bring anything else other than their smartphones to the chamber. The volunteers were asked to stand up and stretch/walk within the chamber for several minutes every hour.

The chamber conditions were set the night before each experiment to ensure that they had reached steady state at the beginning of the experiment. The chamber door was closed during the entire experiment. After the volunteers exited the chamber, the door was kept closed for 30 min and the decay of the NCA concentrations was measured.

Fifteen experiments were performed to investigate NCA emissions from ozone−human chemistry. To demonstrate the influence of ozone on NCA emissions, two types of experiments were performed. In the first type, the volunteers occupied the ozone-free chamber for 3 h and left for a 10 min lunch break, and ozone was added 10 min after the volunteers returned to the chamber for another 2.5 h (ozone from steady state, SS). In the second type of experiments, the target ozone level was established before the volunteers entered the chamber (ozone from start). The volunteers stayed in the chamber for 3 h in the morning, during this time, ozone was

continuously supplied into the chamber. During both types of experiments, the steady-state ozone concentration inside the occupied chamber was around 40 ppb, whereas the target ozone concentration inside the unoccupied chamber was 100 ppb (average actual concentration across all experiments 94 ± 6 ppb).

The impact of clothing on NCA emissions was studied with two sets of loose-fitting clothing; a "long" set consisting of sweatpants, long-sleeve shirt, and calf socks and a "short" set consisting of shorts, t-shirt, and ankle socks. The influence of age on NCA emissions was demonstrated by comparisons between the A2, T4, and S5 groups. Air temperature and relative humidity (RH) in the chamber varied within 26.0−30.3 °C and 18−35%, respectively (Table S1), and their impacts on NCA emissions were investigated as well.

Supplementary experiments were also performed to further validate the findings, including the influence of previously worn clothing, a comparison between clean and worn clothing, and ozone reactions with human exhaled air. Details can be found in Bekö et al.[26]

**Instrumentation and Quality Control.** NCAs in the chamber were sampled at a 2.5 L/min flow rate and measured in real time with a nano condensation nucleus counter (Airmodus A11 nCNC System, Airmodus, Finland), consisting of a particle size magnifier (PSM A10) and a condensation particle counter (CPC A20).[28] The PSM is used to grow small particles to the detectable size range of the CPC with the mixing type principle.[29] The mixing ratio can be changed rapidly, resulting in concomitant size variations in the smallest particles that can be magnified by the PSM. By scanning the mixing ratio continuously, the size distribution of aerosols in the 1−4 nm range can be measured. Relative to other particle detection technologies, such as the scanning mobility particle sizer, this approach minimizes the losses of the smallest aerosols because there is no prior size selection or particle charging. The instrument has been widely applied in atmospheric outdoor NCA measurements and in a limited number of indoor measurements.[3,7] Prior to the campaign, the instrument was fully serviced and calibrated using mono-disperse NiCr oxide particles for the 1−4 nm size range.[26] The PSM ran in the scanning mode with the saturator flow scanning at a constant speed, resulting in the detection of 1.18−4 nm aerosols. A complete scan included two 2 min periods: the saturator flow climbing from 0.1 to 1.3 L/min (upscan) and then decreasing back to 0.1 L/min (downscan). Typically, we averaged aerosol particle concentrations of each size bin measured in the two periods and thus have a time resolution of 4 min. When the variation in NCA concentrations was large, we adopted the 2 min resolution to better capture the NCA dynamics.

The ozone concentration inside the chamber was measured with a time resolution of 10 s with an ozone monitor (Model 205, 2B Technologies, USA) at a 2.0 L/min sampling flow rate. In addition, we also measured real-time air temperature and RH (Vaisala GMW90), concentrations of $CO_2$ (Picarro G2401), $NH_3$ (Picarro G2103), and VOCs (PTR-ToF-MS 8000), and total OH reactivity (customized PTR-MS) inside the chamber. We determined OH concentrations and measured the abundance of squalene in volunteers' skin lipids. Details about the instruments used, placement, and procedures can be found in Figure S1, Section S1 and in Bekö et al.[26]

**Data Analysis.** To obtain real-time NCA concentrations, the raw data files from the A11 nCNC were analyzed using

customized codes in Scilab 6.1.0 software (ESI Group, France) with the stepwise method.[30] The data were corrected for particle losses in the sampling tube (52 cm) due to NCA diffusion onto the tubing wall (penetration efficiency shown in Figure S2). We further aggregated the number concentrations into five size bins (1.18−1.55, 1.55−1.71, 1.71−1.93, 1.93−2.81, and 2.81−4 nm).

The average emission rate of NCA was calculated based on the material-balance equation inside the chamber

$$V\frac{dN_i}{dt} = nE_i - \left(\alpha + \beta_i + \sum_i K_i N_i\right)N_i \qquad (1)$$

where $N_i$ $(cm^{-3})$ is the particle number concentration for particle size $i$; $E_i$ (particles per person-h) is the particle number emission rate per person per hour for particle size $i$; $n$ is the number of occupants; $V$ $(cm^3)$ is the chamber volume; $\alpha$ $(h^{-1})$ is the air change rate; $\beta_i$ $(h^{-1})$ is the particle deposition rate for particle size $i$, obtained via exponential fitting of the particle number concentration during the decay period in each experiment after the volunteers exited the chamber (listed in Table S2, with assumption that the decay rate in the empty chamber represents the deposition rate; see the Discussion section); and $\sum_i K_i N_i$ is the net coagulation sink rate $(h^{-1})$ for the particle population consisting of size $i$, determined following the procedure in Wallace et al.[9] Given the low aerosol particle concentration inside the chamber, the theoretically obtained net coagulation sink rate was as low as $10^{-4}$ to $10^{-3}$ $h^{-1}$,[9,31] which was negligible compared to the air change rate and the particle deposition rate. Thus, for steady-state conditions, we can obtain the average NCA emission rate in each experiment as

$$\overline{E}_i = \frac{V}{n}(\alpha + \beta_i)\overline{N}_i \qquad (2)$$

where the overbar indicates the average values of $E_i$ and $N_i$ during the steady-state period of occupancy. NCA emission rates were normalized by the exposed skin surface area. We estimated the average human body surface area for each group using the height and weight of each volunteer.[32] We assigned the exposed skin fractions as 13.8 and 42.3% of the total body surface area for long and short clothing scenarios, respectively.[33] The normalized NCA emission rates were obtained by dividing the average emission rates by the exposed skin area.

We analyzed Pearson correlations between NCA emissions and measured concentrations of VOCs, $NH_3$, and OH, as well as OH reactivity, to investigate potential NCA formation mechanisms (Table S3). Mann−Whitney and Kruskal−Wallis tests were performed to examine the dependence of NCA emissions on clothing level and age, respectively. The two-tailed test of significance was used.

## ■ RESULTS

**Characteristics of NCA Emissions.** Figure 1 shows a time series of ozone mixing ratio and size-dependent NCA number concentrations in the chamber occupied by young adults (group A2) wearing "long" clothing. During the morning when ozone was absent from the chamber, only a brief increase in the NCA concentrations was observed when the volunteers entered and exited the chamber, presumably caused by the intrusion of air from the corridor through the open door (~5 s). The formation of NCAs was observed in the occupied chamber only after ozone was introduced in the afternoon,
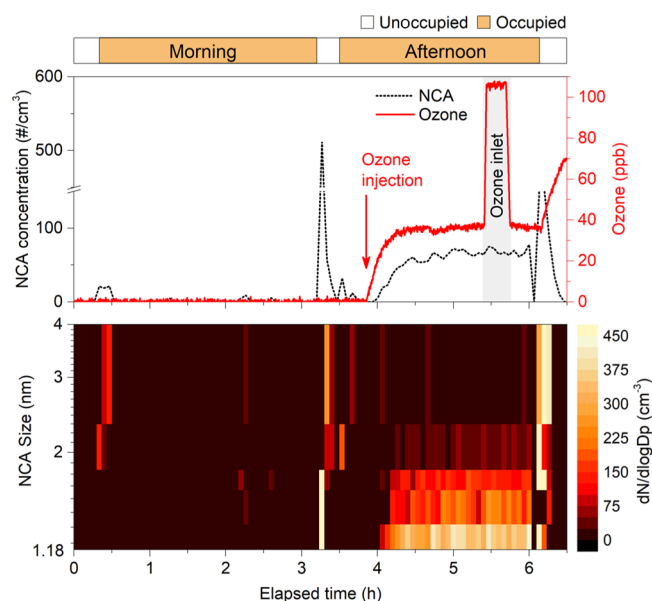


**Figure 1.** Time series of NCA number concentration and ozone (top) and NCA size distribution (bottom). The shown experiment is with young adults (A2) wearing long-sleeve shirts and pants with ozone present from the steady state of human emissions (afternoon). During the period with a gray background, ozone was sampled in the chamber inlet. The NCA size is the activation diameter.

indicating that ozone chemistry was the source of NCAs. The ozone concentration inside the occupied chamber reached a steady-state value of ~40 ppb, which was about 40% of the steady-state ozone concentration in the unoccupied chamber. The concentration of NCAs equilibrated at 60 particles/$cm^3$ 1 h after ozone injection began, with 65% of the measured NCA in the smallest detected size range (1.18−1.55 nm). When the volunteers exited the chamber, the NCA concentration again demonstrated a sudden peak caused by the open chamber door. Afterward, it decreased rapidly to zero due to the removal by ventilation, deposition, and continuous growth, while the ozone concentration increased.

The formation of NCAs began with a time lag relative to the introduction of ozone; it was first detected when the ozone concentration reached 12 ppb, 8 min after ozone introduction had begun (Figure S3a). In another experiment, when the volunteers entered the chamber with ozone at steady state (94 ppb), the NCA formation began instantaneously along with the decrease in the ozone level inside the chamber (Figure S3b). Ozone-initiated human emissions of NCA appear to be limited by the ozone concentration and by the presence of reactive species (e.g., squalene) present on the skin of the volunteers. Moreover, the reaction of ozone with the compounds present on the volunteers' skin is kinetically constrained by the resistance to mass transport across the boundary layer of air adjacent to the surface.[34]

The formation of larger size clusters (2.81−4 nm) also exhibited a time lag relative to the smallest size, 8 min after the appearance of 1.18−1.55 nm aerosols (Figure 1). The time lag suggests that the larger-size NCAs were formed by growth from smaller ones. Previous atmospheric nucleation observations found a size-dependent growth rate ranging from 0.2 to 2.1 nm/h,[35] although the actual values are not comparable to our experiments due to the difference in environmental and chemical conditions. We can presume that in scenarios of low
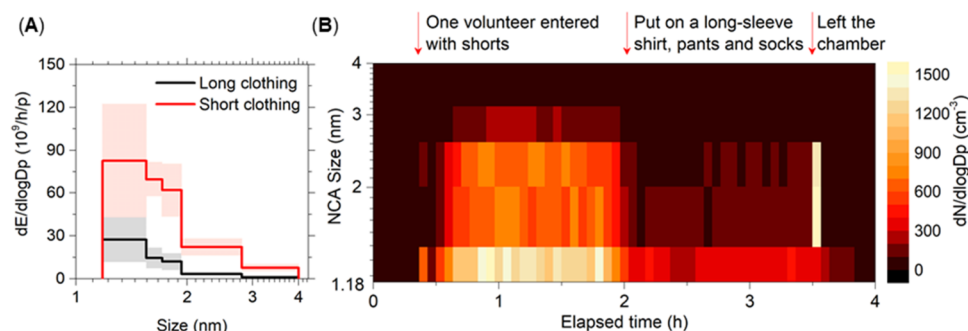
**Figure 2.** Influence of clothing on NCA emissions from ozone−human chemistry. (A) Comparisons of size-resolved NCA emission rates between long and short clothing scenarios. The lines represent averages of all available data within each size bin for the experiments involving young adults A2 ($N = 4$). Shaded areas represent standard deviations; (B) time-series plot of NCA size distribution in the experiment with one volunteer present in the chamber initially bare skinned (shorts only) and then wearing a long-sleeve shirt, pants, and socks donned inside the chamber 90 min after entering the chamber. The clothes were kept in sealed plastic bags inside the chamber before wearing. The NCA size is the activation diameter.
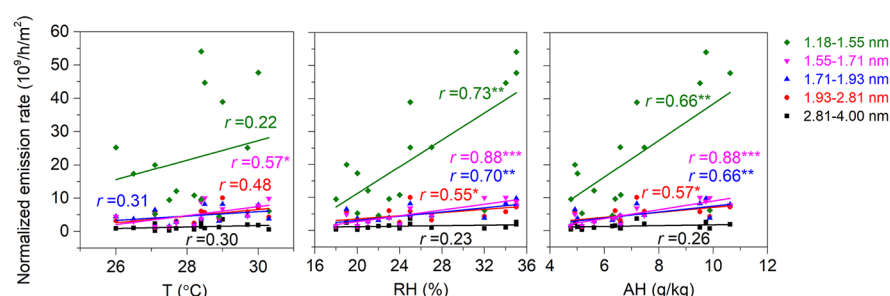


**Figure 3.** Pearson correlation between temperature ($T$), relative humidity (RH) and absolute humidity (AH), and exposed skin-surface-area normalized NCA emission rates for the different NCA size bins. *$p < 0.05$; **$p < 0.01$; and ***$p < 0.001$.

air change rate and/or densely populated environments, the NCAs will reach higher concentrations and subsequently grow over longer time scales to form larger aerosol particles than observed in the present study.

**Influencing Factors.** The NCA emission rates ranged from $2.4 \times 10^9$ to $2.2 \times 10^{10}$ aerosols per person-h, and the exposed-skin-surface-area normalized emission rates were in the range from $9.3 \times 10^9$ to $8.8 \times 10^{10}$ aerosols per h m$^2$ (Table S1). The NCA emissions did not differ significantly ($p = 0.35$) between morning (ozone present from start of the experiment) and afternoon (ozone injected after the steady state was reached in the chamber) hours.

*Clothing.* At similar ozone concentrations in the chamber, young adults emitted about three times more NCAs across all size bins when wearing t-shirt and shorts relative to long-sleeve shirts and pants (Figure 2a). A larger exposed skin surface area provides more opportunity for ozone-skin lipid reactions to occur and less clothing surface to retain NCAs after their release from skin. The skin-surface-area normalized NCA emission rates for experiments with long and short clothing were not significantly different ($p = 0.30$). The substantial influence of clothing on NCA emissions was further demonstrated in a companion experiment with a single bare skinned volunteer in the ozone-laden chamber, who donned long clothing 90 min into the experiment (Figure 2b), substantially decreasing NCA emissions.

*Temperature and RH.* There was a positive but barely significant correlation between air temperature and normalized NCA emissions (Figure 3). This may reflect increased ammonia emission rate with temperature,[36] which will be discussed later. The rate of increase in NCA emission with a unit change in temperature decreased with increasing particle size. Increasing temperature generally accelerates chemical reactions in the air, which can lead to more rapid aerosol particle formation, as reactive volatiles are oxidized to large, polar species that are prone to condensation.[37] On the other hand, air temperature also influences the partitioning of organics between the gas phase and the condensed phase, with more being present in the gas phase at elevated temperature.[38,39] Both RH and absolute humidity (AH) were positively correlated with normalized NCA emission rates; the relationship was significant for all but the largest size bin. The emission rates increased with humidity more rapidly for smaller NCAs. Such a positive correlation could reflect the hygroscopicity of the formed NCAs and the importance of water in stabilizing the initial cluster. In addition, at higher humidity, condensed-phase ozonolysis products shift from secondary ozonides to carbonyls so that the concentrations of gas-phase oxidation products increase.[20,40] However, it should be noted that the range of temperature and RH used in this study is relatively narrow (26.0−30.3 °C and 18−35%).

*Age.* Teenagers exposed to ozone emitted about 2−3× more NCAs than seniors and young adults wearing long clothing, respectively (Figure 4). Larger amounts of squalene and cholesterol were measured in teenagers' skin lipids compared to the other two age groups (mean squalene per 100 cm$^2$ wiped area: teenagers $223 \pm 133$ $\mu$g, seniors $32 \pm 27$ $\mu$g, and young adults $189 \pm 84$ $\mu$g). The RH was about 10% higher during the experiments with teenagers compared to the rest of the experiments, which could have contributed to the stronger NCA signals. We suspect that the higher NCA emissions from seniors compared with young adults despite their lower content of squalene in their skin oil may be attributed to the larger wrinkle areas, increased skin roughness,
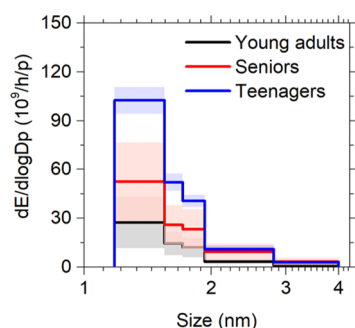
**Figure 4.** Influence of age on NCA emissions from ozone–human chemistry. The lines represent averages of all available data within each size bin for the experiments involving young adults A2 ($N = 4$), seniors S5 ($N = 3$), and teenagers T4 ($N = 3$), all wearing long clothing. Shaded areas represent standard deviations. The NCA size is the activation diameter.

and thus larger skin surface area available for ozone reactions among seniors.[41] Age-dependent skin lipid composition may also contribute to the difference,[42] which merits further research attention.

## DISCUSSION

**Potential Mechanisms of NCA Formation.** Ozone reacts with chemical constituents of exhaled air,[43] skin lipids,[18] personal-care products,[44] and clothing fabric.[19,22] The use of personal-care products was strictly limited in this study, so its contribution to the NCA formation was negligible. Human exhaled air contains isoprene,[43] which can react with ozone to form secondary organic aerosols (SOAs) albeit at relatively low yield.[45] However, the pseudo-first-order rate constant for this reaction is much smaller than the ventilation rate used in our experiments (0.04 h$^{-1}$ vs 3.2 h$^{-1}$). During a companion experiment to investigate the ozone reaction with human exhaled air, the volunteers were seated in the neighboring auxiliary chamber and exhaled through breathing masks into the primary chamber where the measurements took place.[26] Ozone concentration reached a stable level at ~90 ppb soon after its generation began. Indeed, we did not detect NCAs during the co-occurring presence of ozone and exhaled air.

The liquid crystal display (LCD) screens of smartphones and tablets can also emit unsaturated VOCs, albeit at a considerably lower rate relative to humans.[46] Four tablets were continuously present inside the chamber, including during ozone-rich unoccupied periods. No NCA signals were detected during this time. In addition, the pseudo-first-order rate constants of LCD-emitted unsaturated VOCs were significantly lower than the air change rate (<0.1 h$^{-1}$ vs 3.2 h$^{-1}$).[46] Therefore, it is unlikely that the VOC emissions from LCD screens of the devices contributed to NCA emissions in this study. While the reactions of ozone with the surface of clean clothing (without human present) can produce VOCs,[19] they did not generate NCAs (Figure S4). On the other hand, when previously worn clothing containing skin lipids was placed in the chamber in the presence of ozone, a clear NCA signal was detected (Figure S4). These observations strongly suggest that ozone reactions with human skin lipids are responsible for the observed NCA emissions.

Skin lipids contain organic compounds such as squalene and unsaturated fatty acids,[47] which can react rapidly with ozone by virtue of their double bonds. The ozonolysis products include gaseous compounds (e.g., acetone, geranyl acetone, 6-methyl-5-hepten-2-one (6MHO), 4-oxopentanal (4OPA), hexanal, and decanal), as well as compounds with low volatility (C17-trienoic acid, C17-trienal, and C22-tetraenoic acid).[18] Based
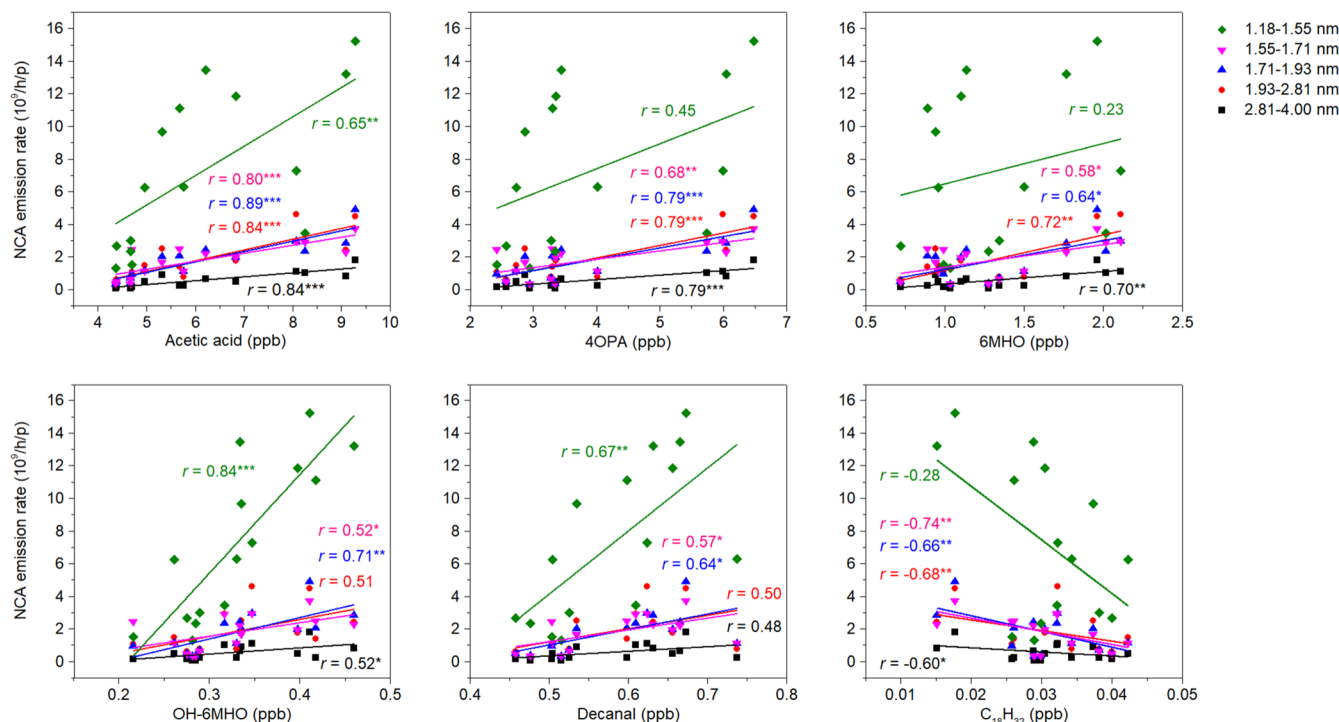


**Figure 5.** Pearson correlations between steady-state concentrations of selected organic compounds (acetic acid, 4OPA, 6MHO, OH-6MHO, decanal, and a compound or fragment with molecular formula $C_{18}H_{32}$) and NCA emissions of different sizes across all experiments. *$p < 0.05$; **$p < 0.01$; and ***$p < 0.001$.

on prior studies,[48−50] we anticipate that these low-volatility products generated by reactions of ozone with unsaturated skin lipids contribute to the formation of NCAs. We quantified squalene in the skin wipe samples collected from six volunteers. The mostly positive correlations between the amount of squalene in skin wipes and skin-surface-area normalized NCA emission rates (Figure S5) further underline the assumption that the ozonolysis of organic compounds present in skin lipids is the major driving mechanism of the NCA formations.

Figure 5 shows that the NCA emissions in most size ranges significantly positively correlated with the steady-state concentrations of the ozonolysis products acetic acid, 4OPA, 6MHO, OH-6MHO, and decanal across all experiments. Also shown is a plot for a $C_{18}H_{32}$ hydrocarbon that demonstrated a negative correlation with NCA emissions. This is just one example from a series including $C_{17}H_n$, $C_{18}H_n$, $C_{19}H_n$, and $C_{20}H_n$ hydrocarbons that are all anticorrelated with NCA emissions (see Table S3). The PTR-ToF-MS identifies only the molecular formula based on the exact mass determination of these species; we are unable to identify their structures unequivocally. They could be unsaturated linear, branched, or cyclic hydrocarbons. Alternatively, they could be fragments produced when water is lost from protonated oxygenated precursors. We suspect the latter (fragments of oxygenated precursors), since the corresponding saturated hydrocarbons ($C_{17}H_{36}$, $C_{18}H_{38}$, $C_{19}H_{40}$, or $C_{20}H_{42}$) were not identified. Furthermore, in an ozone-rich environment, a fragment of an oxidation product makes more sense than an unsaturated hydrocarbon (which would react with ozone). Regardless, a larger concentration of NCAs in the chamber translates to a larger fraction of C17, C18, C19, and C20 organic compounds partitioning onto NCAs, lowering the gas-phase concentrations of these low-volatility species as measured by the PTR-ToF-MS. The full correlation matrix for the NCA emissions and detected gas-phase organic compounds is presented in Table S3.

Some primary products of skin lipid ozonolysis contain unsaturated carbon−carbon bonds that can subsequently react with ozone and form secondary products. For example, 6MHO and OH-6MHO originate from both primary and secondary chemistry, while 4OPA is a product of secondary ozone reactions only (Figure S6).[18] Figure 6 shows an example of a time series for primary and secondary reaction products along with ozone and NCA concentrations. The concentration of 6MHO followed the pattern of ozone concentrations, reaching steady state ∼1 h after ozone dosing began. In contrast, the concentration of 4OPA increased during the course of the experiment and did not reach steady state. The NCA curve in Figure 6 is shaped similar to that of ozone, reaching steady state ∼0.5 h after initiation. Additionally, NCA concentrations correlated better with the concentrations of 6MHO than 4OPA (correlation coefficient: 0.98 vs 0.87). This suggests that for NCA formation in these experiments, primary ozone-skin lipid chemistry may be of more importance than secondary chemistry, which takes longer to attain steady state.

Primary ozone-initiated chemistry takes place mainly on the surfaces of the skin and worn clothing. Secondary reactions occur both on the surfaces and in the gas phase. After the volunteers exited the chamber, ozone concentration increased and the concentrations of the gas-phase reaction products and $CO_2$ decreased. The decay rates of these compounds varied. The concentration of 6MHO decayed much faster than $CO_2$;
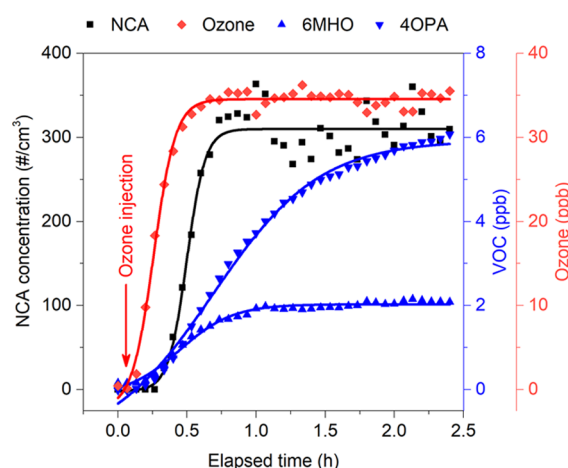


**Figure 6.** Time series of NCA, ozone, 6MHO, and 4OPA concentrations. Data are from the experiment with young adults (A2) wearing t-shirts and shorts with ozone dosed after human emissions reached steady state (afternoon). Boltzmann equation was applied for curve fitting (solid lines).

neither compound had sources present, and 6MHO continued to react with ozone. Lower decay rates were observed for 4OPA and acetic acid, reflecting the fact that these compounds continued to be formed by residual reactions (Figure S7). However, it remains uncertain whether the residual reactions generated NCAs, as the clusters quickly disappeared (large decay rates). It is therefore also unclear whether the decay rates reliably reflect NCA deposition loss rates (Table S2), although the values were within the range reported from theoretical calculations (Figure S8).[51] The relative contribution of surface reactions and gas-phase reactions to the observed NCA warrants further investigation.

Another means of producing NCAs is through OH radical oxidation. Criegee intermediates formed during ozonolysis decompose to produce OH radicals.[52] OH radicals can oxidize saturated and unsaturated organic compounds at a rapid rate. Reactions occur both in the gas phase and on surfaces and can produce products with volatilities lower than those of the precursors,[49,53] contributing to the formation of SOAs.[54] Interestingly, the normalized NCA emissions were negatively correlated with OH concentration in the chamber (Table S3). When ozone reacts with human skin surface lipids, Criegee intermediates that might otherwise have decomposed to yield OH radicals may instead react with aldehydes and acids produced by ozone/skin oil chemistry. The consequent hydroperoxides may play a role in NCA formation. Alternatively, NCA formation may consume OH at a faster rate relative to the production of OH during ozonolysis. Regardless, significant positive correlations were found between skin-surface-area normalized NCA emissions and total OH reactivity (Table S3), as both increase with increasing ozone−human interaction.

Humans are substantial emitters of ammonia ($NH_3$), in particular through the skin. Throughout the experiments, we observed significant $NH_3$ emissions from the volunteers; emission rates were higher at elevated temperatures and with a larger unclothed skin surface area.[36] Previous studies have indicated that the presence of $NH_3$ can enhance SOA formation resulting from ozone−terpene reactions.[55,56] This has been interpreted as the stabilization of the initial molecular cluster against separation by the presence of ammonia.[57] Gas-

phase reactions between $NH_3$ and mono-, oxo-, and di-carboxylic acids, formed when ozone reacts with squalene and unsaturated fatty acids in human skin oil,[18] may contribute to NCAs via the formation of condensable salts. Amines, although present at concentrations several orders of magnitude lower than $NH_3$, may also play a role.[25,35,58] Emissions of NCAs in several size bins were significantly positively correlated with glycine ($C_2H_5NO_2$), succinimide ($C_4H_5NO_2$), and cyclohexyl-prop-2-ynyl-amine ($C_9H_{15}N$, Table S3). Such a chemical process involving acids and $NH_3$/amines has been identified as an important pathway to form atmospheric clusters.[59,60]

The concentration of nitric oxide (NO) was expected to be low during these chamber experiments, especially when ozone was present. Under such conditions, the lifetimes of alkylperoxy radicals ($RO_2^\bullet$), derived from ozone-initiated chemistry, are relatively long and autoxidation reactions can generate highly oxidized multifunctional (HOM) compounds.[61] Autoxidation of limonene has recently been reported to occur in a university art museum when NO concentrations were low.[62] Furthermore, Criegee intermediates formed during ozonolysis, have been shown to propagate chain reactions in the autoxidation of unsaturated lipids.[63] Autoxidation reactions and consequent HOMs are still another potential contributor to the formation of NCAs observed in the present study, as has been found in the outdoor atmosphere.[60]

The aforementioned chemistry is associated most closely with aerosols of the smallest size bin, as larger clusters are likely to originate from the growth of the smaller ones via physical processes such as coagulation and condensation. If we assume, for example, OH-geranyl acetone ($C_{13}H_{22}O_2$, one of the squalene ozonolysis products) as a constituent of the formed clusters, the 1.18−1.55 nm NCA would be formed by 3−4 molecules, whereas 4 and 12 times more molecules are required to form 2−3 and 3−4 nm clusters, respectively (see Section S2 for details). This may also explain the higher concentrations in the smaller size bins and the delayed signals of larger clusters shown in Figure 1. Future research is warranted to investigate the chemical and physical processes, in both particle and gas phases, involved in the growth of NCAs generated by ozone−human chemistry over longer residence times than those accessed at this ventilation rate.

**Limitations.** Replicate experiments demonstrated reasonable reproducibility of the results (mostly within 40%) considering the factors influencing the measurements. The exceptions were the experiments on 8 and 10 April, where a fourfold difference in the normalized NCA emission rate was observed. NCA concentrations as low as in this study (10 to 100 aerosols/cm$^3$) are sensitive to small differences in the available precursors (skin lipids and ozone), the possible air disturbances induced by human volunteers in the chamber, the state of the chamber surfaces, and the overall initial conditions. Furthermore, uncertainties associated with the NCA measurement instrument should also be considered, which were around 50% given the concentrations.[6] As proposed by Chan et al.,[64] the stepwise data inversion method used in this study might result in overestimated sub-3 nm NCA concentrations in scenarios with high concentrations of larger particles and strong concentration fluctuations. However, given the stable NCA concentrations (Figure 1) and low 10−1000 nm particle levels (Figure S9) in this study, uncertainties associated with the data inversion method are expected to be negligible. The limit of detection for the 14 VOCs for which the PTR-ToF-MS was calibrated with a gas standard ranged from 7 to 171 ppt.

Other VOCs were quantified with an accuracy around 50%. See Wang et al.[65] for additional details on the accuracy of the chemical measurements. Another limitation of this study is the lack of continuous aerosol size distribution measurements beyond the NCA mode (4−10 nm). Future measurements should comprehensively cover the relevant particle size range in order to study the growth of NCA particles into larger sizes and the associated particle dynamics.

**Implications and Future Outlook.** Humans significantly contribute to the chemical and particulate composition of indoor environments. Ozone-initiated chemical transformations play an important role in this. We observed for the first time the formation of single-digit nanometer-size aerosols resulting from ozone−human chemistry. Although the NCA emission rates from ozone chemistry continuously occurring on humans in this study were 2−3 orders of magnitude lower than from other known sporadic indoor NCA sources, including cooking[7] and 3D printers,[10] the results provide new insights into NCA formation in our immediate vicinity when encountering ozone. The findings highlight the interconnected nature of gas-phase and particle-phase components of indoor air, as well as their dynamics. Further investigations into the chemical processes driving NCA formation are warranted, especially over longer residence times, including the contribution of primary and secondary reactions, the role of OH radicals, $NH_3$, and other chemicals, and the fate of the resulting NCA.

The present study was performed in a well-controlled stainless-steel climate chamber with efficient filtration. The air in real indoor environments contains various additional organic and inorganic compounds in both the gas phase and on surfaces. Some of these are anticipated to participate in the formation of NCAs and alter the properties of the newly formed aerosols. Furthermore, skin oils and their chemical constituents can be found on various indoor surfaces, such as glass, carpet, and settled dusts.[66,67] NCA formation from human−ozone interaction may therefore be substantially more pronounced in real indoor environments. On the other hand, the presence of other aerosol sources could act as larger coagulation/condensation sinks for the NCA and gas-phase precursors and thus limit the nucleation of NCA in real indoor environments. Therefore, the formation of NCA in indoor environments is likely a complex multigenerational process, the understanding of which requires further investigations.

The approximately 100 ppb inlet ozone concentration, analogous to the ozone concentration outside a building, is similar to what might occur during a pollution episode in an urban area on a hot day. The ∼40 ppb ozone level in the occupied chamber has been measured in buildings with high ventilation rates during ozone pollution episodes.[68] It should be noted that indoor ozone levels are strongly dependent on outdoor ozone concentrations, ventilation, and indoor ozone sources/sinks[69,70] and thus vary in indoor environments.[71,72] Future research on the influence of ozone concentration on human-derived NCA emissions is warranted.

Finally, ozone−human chemistry has the potential to contribute to near-ground atmospheric NCA formation, especially in ozone-polluted and crowded urban areas. In summer, higher ozone concentrations, temperatures, humidity, and shorter clothing may lead to elevated NCA generation, with potentially meaningful contribution to outdoor SOA production.

## ASSOCIATED CONTENT

### ⓢ Supporting Information

The Supporting Information is available free of charge at https://pubs.acs.org/doi/10.1021/acs.est.1c03379.

Details of measurement instruments and procedures; estimation of the number of molecules constituting NCAs of different sizes; schematic layout of the unoccupied environmental chamber with sampling locations; penetration efficiency due to particle diffusional losses in the sampling tube; time series of NCA number concentrations and ozone in the experiment; time series of NCA distribution in the chamber with ozone and either new or worn clothing; Pearson correlation between squalene in skin wipes and NCA emission rates across different NCA size ranges; example of primary and secondary reactions during squalene ozonolysis; decay rates of acetic acid, 4OPA, 6MHO, $CO_2$, and NCA; comparison between obtained NCA decay rates and those in earlier theoretical calculations; steady-state 1−1000 nm particle size distribution; summary of experimental conditions and associated NCA number concentrations and emission rates; empirically derived size-resolved decay rates; and Pearson correlations between NCA emission rates and steady-state VOC concentrations, OH reactivity, OH concentrations, and $NH_3$ concentrations (PDF)

## AUTHOR INFORMATION

### Corresponding Authors

**Dusan Licina** − Human-Oriented Built Environment Lab, School of Architecture, Civil and Environmental Engineering, École Polytechnique Fédérale de Lausanne (EPFL), Lausanne 1015, Switzerland; ⓞ orcid.org/0000-0001-5945-0872; Email: dusan.licina@epfl.ch

**Gabriel Bekö** − International Centre for Indoor Environment and Energy, Department of Civil Engineering, Technical University of Denmark, Kongens Lyngby 2800, Denmark; ⓞ orcid.org/0000-0001-6107-8336; Email: gab@byg.dtu.dk

### Authors

**Shen Yang** − Human-Oriented Built Environment Lab, School of Architecture, Civil and Environmental Engineering, École Polytechnique Fédérale de Lausanne (EPFL), Lausanne 1015, Switzerland

**Charles J. Weschler** − International Centre for Indoor Environment and Energy, Department of Civil Engineering, Technical University of Denmark, Kongens Lyngby 2800, Denmark; Environmental and Occupational Health Sciences Institute, Rutgers University, Piscataway, New Jersey 08854, United States; ⓞ orcid.org/0000-0002-9097-5850

**Nijing Wang** − Max Planck Institute for Chemistry, Mainz 55128, Germany; ⓞ orcid.org/0000-0003-3197-8151

**Nora Zannoni** − Max Planck Institute for Chemistry, Mainz 55128, Germany; ⓞ orcid.org/0000-0003-2721-5362

**Mengze Li** − Max Planck Institute for Chemistry, Mainz 55128, Germany; ⓞ orcid.org/0000-0003-0620-6301

**Joonas Vanhanen** − Airmodus Limited, Helsinki FI-00560, Finland

**Sarka Langer** − IVL Swedish Environmental Research Institute, Göteborg SE-400 14, Sweden; Department of Architecture and Civil Engineering, Division of Building Services Engineering, Chalmers University of Technology, Göteborg SE-412 96, Sweden; ⓞ orcid.org/0000-0002-6580-8911

**Pawel Wargocki** − International Centre for Indoor Environment and Energy, Department of Civil Engineering, Technical University of Denmark, Kongens Lyngby 2800, Denmark

**Jonathan Williams** − Max Planck Institute for Chemistry, Mainz 55128, Germany; Energy, Environment and Water Research Center, The Cyprus Institute, Nicosia 2121, Cyprus; ⓞ orcid.org/0000-0001-9421-1703

Complete contact information is available at:
https://pubs.acs.org/10.1021/acs.est.1c03379

### Notes

The authors declare no competing financial interest.

## ACKNOWLEDGMENTS

## REFERENCES

(1) Rönkkö, T.; Kuuluvainen, H.; Karjalainen, P.; Keskinen, J.; Hillamo, R.; Niemi, J. v.; Pirjola, L.; Timonen, H. J.; Saarikoski, S.; Saukko, E.; Järvinen, A.; Silvennoinen, H.; Rostedt, A.; Olin, M.; Yli-Ojanperä, J.; Nousiainen, P.; Kousa, A.; Dal Maso, M. Traffic is a major source of atmospheric nanocluster aerosol. *Proc. Natl. Acad. Sci. U.S.A.* **2017**, *114*, 7549−7554.

(2) Jokinen, T.; Sipilä, M.; Kontkanen, J.; Vakkari, V.; Tisler, P.; Duplissy, E.-M.; Junninen, H.; Kangasluoma, J.; Manninen, H. E.; Petäjä, T.; Kulmala, M.; Worsnop, D. R.; Kirkby, J.; Virkkula, A.; Kerminen, V.-M. Ion-induced sulfuric acid-ammonia nucleation drives particle formation in coastal Antarctica. *Sci. Adv.* **2018**, *4*, No. eaat9744.

(3) Kontkanen, J.; Lehtipalo, K.; Ahonen, L.; Kangasluoma, J.; Manninen, H. E.; Hakala, J.; Rose, C.; Sellegri, K.; Xiao, S.; Wang, L.; Qi, X.; Nie, W.; Ding, A.; Yu, H.; Lee, S.; Kerminen, V.-M.; Petäjä, T.; Kulmala, M. Measurements of sub-3 nm particles using a particle size magnifier in different environments: from clean mountain top to polluted megacities. *Atmos. Chem. Phys.* **2017**, *17*, 2163−2187.

(4) Kulmala, M.; Riipinen, I.; Sipila, M.; Manninen, H. E.; Petaja, T.; Junninen, H.; Maso, M. D.; Mordas, G.; Mirme, A.; Vana, M.; Hirsikko, A.; Laakso, L.; Harrison, R. M.; Hanson, I.; Leung, C.; Lehtinen, K. E. J.; Kerminen, V.-M. Toward Direct Measurement of Atmospheric Nucleation. *Science* **2007**, *318*, 89−92.

(5) Lee, S.-H.; Gordon, H.; Yu, H.; Lehtipalo, K.; Haley, R.; Li, Y.; Zhang, R. New particle formation in the atmosphere: from molecular clusters to global climate. *J. Geophys. Res.: Atmos.* **2019**, *124*, 7098−7146.

(6) Kangasluoma, J.; Cai, R.; Jiang, J.; Deng, C.; Stolzenburg, D.; Ahonen, L. R.; Chan, T.; Fu, Y.; Kim, C.; Laurila, T. M.; Zhou, Y.; Dada, L.; Sulo, J.; Flagan, R. C.; Kulmala, M.; Petäjä, T.; Lehtipalo, K. Overview of measurements and current instrumentation for 1−10 nm aerosol particle number size distributions. *J. Aerosol Sci.* **2020**, *148*, 105584.

(7) Patel, S.; Sankhyan, S.; Boedicker, E. K.; Decarlo, P. F.; Farmer, D. K.; Goldstein, A. H.; Katz, E. F.; Nazaroff, W. W.; Tian, Y.; Vanhanen, J.; Vance, M. E. Indoor particulate matter during HOMEChem: concentrations, size distributions, and exposures. *Environ. Sci. Technol.* **2020**, *54*, 7107−7116.

(8) Wallace, L.; Wang, F.; Howard-Reed, C.; Persily, A. Contribution of gas and electric stoves to residential ultrafine particle

concentrations between 2 and 64 nm: Size distributions and emission and coagulation rates. *Environ. Sci. Technol.* **2008**, *42*, 8641–8647.

(9) Wallace, L.; Jeong, S. G.; Rim, D. Dynamic behavior of indoor ultrafine particles (2.3-64 nm) due to burning candles in a residence. *Indoor Air* **2019**, *29*, 1018–1027.

(10) Poikkimäki, M.; Koljonen, V.; Leskinen, N.; Närhi, M.; Kangasniemi, O.; Kausiala, O.; Dal Maso, M. Nanocluster aerosol emissions of a 3D printer. *Environ. Sci. Technol.* **2019**, *53*, 13618–13628.

(11) Wallace, L. A.; Ott, W. R.; Weschler, C. J.; Lai, A. C. K. Desorption of SVOCs from heated surfaces in the form of ultrafine particles. *Environ. Sci. Technol.* **2017**, *51*, 1140–1146.

(12) Schraufnagel, D. E. The health effects of ultrafine particles. *Exp. Mol. Med.* **2020**, *52*, 311–317.

(13) Carnerero, C.; Pérez, N.; Petäjä, T.; Laurila, T. M.; Ahonen, L. R.; Kontkanen, J.; Ahn, K.-H.; Alastuey, A.; Querol, X. Relating high ozone, ultrafine particles, and new particle formation episodes using cluster analysis. *Atmos. Environ.: X* **2019**, *4*, 100051.

(14) Nazaroff, W. W.; Weschler, C. J.; Corsi, R. L. Indoor air chemistry and physics. *Atmos. Environ.* **2003**, *37*, 5451–5453.

(15) Yang, S.; Perret, V.; Hager Jörin, C.; Niculita-Hirzel, H.; Goyette Pernot, J.; Licina, D. Volatile organic compounds in 169 energy-efficient dwellings in Switzerland. *Indoor Air* **2020**, *30*, 481–491.

(16) Weschler, C. J.; Carslaw, N. Indoor Chemistry. *Environ. Sci. Technol.* **2018**, *52*, 2419–2428.

(17) Weschler, C. J. Roles of the human occupant in indoor chemistry. *Indoor Air* **2016**, *26*, 6–24.

(18) Wisthaler, A.; Weschler, C. J. Reactions of ozone with human skin lipids: Sources of carbonyls, dicarbonyls, and hydroxycarbonyls in indoor air. *Proc. Natl. Acad. Sci. U.S.A.* **2010**, *107*, 6568–6575.

(19) Yang, S.; Gao, K.; Yang, X. Volatile organic compounds (VOCs) formation due to interactions between ozone and skin-oiled clothing: Measurements by extraction-analysis-reaction method. *Build. Environ.* **2016**, *103*, 146–154.

(20) Arata, C.; Heine, N.; Wang, N.; Misztal, P. K.; Wargocki, P.; Bekö, G.; Williams, J.; Nazaroff, W. W.; Wilson, K. R.; Goldstein, A. H. Heterogeneous ozonolysis of squalene: Gas-phase products depend on water vapor concentration. *Environ. Sci. Technol.* **2019**, *53*, 14441–14448.

(21) Zhou, S.; Forbes, M. W.; Abbatt, J. P. D. Kinetics and products from heterogeneous oxidation of squalene with ozone. *Environ. Sci. Technol.* **2016**, *50*, 11688–11697.

(22) Rai, A. C.; Guo, B.; Lin, C.-H.; Zhang, J.; Pei, J.; Chen, Q. Ozone reaction with clothing and its initiated particle generation in an environmental chamber. *Atmos. Environ.* **2013**, *77*, 885–892.

(23) Xiang, J.; Weschler, C. J.; Mo, J.; Day, D.; Zhang, J.; Zhang, Y. Ozone, electrostatic precipitators, and particle number concentrations: correlations observed in a real office during working hours. *Environ. Sci. Technol.* **2016**, *50*, 10236–10244.

(24) Stolzenburg, D.; Fischer, L.; Vogel, A. L.; Heinritzi, M.; Schervish, M.; Simon, M.; Wagner, A. C.; Dada, L.; Ahonen, L. R.; Amorim, A.; Baccarini, A.; Bauer, P. S.; Baumgartner, B.; Bergen, A.; Bianchi, F.; Breitenlechner, M.; Brilke, S.; Buenrostro Mazon, S.; Chen, D.; Dias, A.; Draper, D. C.; Duplissy, J.; el Haddad, I.; Finkenzeller, H.; Frege, C.; Fuchs, C.; Garmash, O.; Gordon, H.; He, X.; Helm, J.; Hofbauer, V.; Hoyle, C. R.; Kim, C.; Kirkby, J.; Kontkanen, J.; Kürten, A.; Lampilahti, J.; Lawler, M.; Lehtipalo, K.; Leiminger, M.; Mai, H.; Mathot, S.; Mentler, B.; Molteni, U.; Nie, W.; Nieminen, T.; Nowak, J. B.; Ojdanic, A.; Onnela, A.; Passananti, M.; Petäjä, T.; Quéléver, L. L. J.; Rissanen, M. P.; Sarnela, N.; Schallhart, S.; Tauber, C.; Tomé, A.; Wagner, R.; Wang, M.; Weitz, L.; Wimmer, D.; Xiao, M.; Yan, C.; Ye, P.; Zha, Q.; Baltensperger, U.; Curtius, J.; Dommen, J.; Flagan, R. C.; Kulmala, M.; Smith, J. N.; Worsnop, D. R.; Hansel, A.; Donahue, N. M.; Winkler, P. M. Rapid growth of organic aerosol nanoparticles over a wide tropospheric temperature range. *Proc. Natl. Acad. Sci. U.S.A.* **2018**, *115*, 9122–9127.

(25) Wang, M.; Kong, W.; Marten, R.; He, X.-C.; Chen, D.; Pfeifer, J.; Heitto, A.; Kontkanen, J.; Dada, L.; Kürten, A.; Yli-Juuti, T.; Manninen, H. E.; Amanatidis, S.; Amorim, A.; Baalbaki, R.; Baccarini, A.; Bell, D. M.; Bertozzi, B.; Bräkling, S.; Brilke, S.; Murillo, L. C.; Chiu, R.; Chu, B.; de Menezes, L.-P.; Duplissy, J.; Finkenzeller, H.; Carracedo, L. G.; Granzin, M.; Guida, R.; Hansel, A.; Hofbauer, V.; Krechmer, J.; Lehtipalo, K.; Lamkaddam, H.; Lampimäki, M.; Lee, C. P.; Makhmutov, V.; Marie, G.; Mathot, S.; Mauldin, R. L.; Mentler, B.; Müller, T.; Onnela, A.; Partoll, E.; Petäjä, T.; Philippov, M.; Pospisilova, V.; Ranjithkumar, A.; Rissanen, M.; Rörup, B.; Scholz, W.; Shen, J.; Simon, M.; Sipilä, M.; Steiner, G.; Stolzenburg, D.; Tham, Y. J.; Tomé, A.; Wagner, A. C.; Wang, D. S.; Wang, Y.; Weber, S. K.; Winkler, P. M.; Wlasits, P. J.; Wu, Y.; Xiao, M.; Ye, Q.; Zauner-Wieczorek, M.; Zhou, X.; Volkamer, R.; Riipinen, I.; Dommen, J.; Curtius, J.; Baltensperger, U.; Kulmala, M.; Worsnop, D. R.; Kirkby, J.; Seinfeld, J. H.; El-Haddad, I.; Flagan, R. C.; Donahue, N. M. Rapid growth of new atmospheric particles by nitric acid and ammonia condensation. *Nature* **2020**, *581*, 184–189.

(26) Bekö, G.; Wargocki, P.; Wang, N.; Li, M.; Weschler, C. J.; Morrison, G.; Langer, S.; Ernle, L.; Licina, D.; Yang, S.; Zannoni, N.; Williams, J. The Indoor Chemical Human Emissions and Reactivity (ICHEAR) project: Overview of experimental methodology and preliminary results. *Indoor Air* **2020**, *30*, 1213–1228.

(27) Yang, S.; Bekö, G.; Wargocki, P.; Williams, J.; Licina, D. Human emissions of size-resolved fluorescent aerosol particles: Influence of personal and environmental factors. *Environ. Sci. Technol.* **2021**, *55*, 509–518.

(28) Vanhanen, J.; Mikkilä, J.; Lehtipalo, K.; Sipilä, M.; Manninen, H. E.; Siivola, E.; Petäjä, T.; Kulmala, M. Particle size magnifier for nano-CN detection. *Aerosol Sci. Technol.* **2011**, *45*, 533–542.

(29) McMurry, P. H. The history of condensation nucleus counters. *Aerosol Sci. Technol.* **2000**, *33*, 297–322.

(30) Lehtipalo, K.; Leppä, J.; Kontkanen, J.; Kangasluoma, J.; Franchin, A.; Wimnner, D.; Schobesberger, S.; Junninen, H.; Petäjä, T.; Sipilä, M.; Mikkilä, J.; Vanhanen, J.; Worsnop, D. R.; Kulmala, M. Methods for determining particle size distribution and growth rates between 1 and 3 nm using the Particle Size Magnifier. *Boreal Environ. Res.* **2014**, *19*, 215–236.

(31) Alam, M. K. The effect of van der Waals and viscous forces on aerosol coagulation. *Aerosol Sci. Technol.* **1987**, *6*, 41–52.

(32) du Bois, D.; du Bois, E. F. A formula to estimate the approximate surface area if height and weight be known. *Arch. Intern. Med.* **1916**, *XVII*, 863–871.

(33) Lee, J.-Y.; Choi, J.-W. Estimation of regional body surface area covered by clothing. *J. Hum. Environ. Stud.* **2009**, *12*, 35–45.

(34) Salvador, C. M.; Bekö, G.; Weschler, C. J.; Morrison, G.; le Breton, M.; Hallquist, M.; Ekberg, L.; Langer, S. Indoor ozone/human chemistry and ventilation strategies. *Indoor Air* **2019**, *29*, 913–925.

(35) Kulmala, M.; Kontkanen, J.; Junninen, H.; Lehtipalo, K.; Manninen, H. E.; Nieminen, T.; Petäjä, T.; Sipilä, M.; Schobesberger, S.; Rantala, P.; Franchin, A.; Jokinen, T.; Järvinen, E.; Äijälä, M.; Kangasluoma, J.; Hakala, J.; Aalto, P. P.; Paasonen, P.; Mikkilä, J.; Vanhanen, J.; Aalto, J.; Hakola, H.; Makkonen, U.; Ruuskanen, T.; Mauldin, R. L.; Duplissy, J.; Vehkamäki, H.; Bäck, J.; Kortelainen, A.; Riipinen, I.; Kurtén, T.; Johnston, M. v.; Smith, J. N.; Ehn, M.; Mentel, T. F.; Lehtinen, K. E. J.; Laaksonen, A.; Kerminen, V.-M.; Worsnop, D. R. Direct observations of atmospheric aerosol nucleation. *Science* **2013**, *339*, 943–946.

(36) Li, M.; Weschler, C. J.; Bekö, G.; Wargocki, P.; Lucic, G.; Williams, J. Human ammonia emission rates under various indoor environmental conditions. *Environ. Sci. Technol.* **2020**, *54*, 5419–5428.

(37) Zeng, G.; Holladay, S.; Langlois, D.; Zhang, Y.; Liu, Y. Kinetics of heterogeneous reaction of ozone with linoleic acid and its dependence on temperature, physical state, RH, and ozone concentration. *J. Phys. Chem. A* **2013**, *117*, 1963–1974.

(38) Chen, H.; Finlayson-Pitts, B. J. New particle formation from methanesulfonic acid and amines/ammonia as a function of temperature. *Environ. Sci. Technol.* **2017**, *51*, 243–252.

(39) Sheehan, P. E.; Bowman, F. M. Estimated effects of temperature on secondary organic aerosol concentrations. *Environ. Sci. Technol.* **2001**, *35*, 2129−2135.

(40) Heine, N.; Houle, F. A.; Wilson, K. R. Connecting the elementary reaction pathways of Criegee intermediates to the chemical erosion of squalene interfaces during ozonolysis. *Environ. Sci. Technol.* **2017**, *51*, 13740−13748.

(41) Manuskiatti, W.; Schwindt, D. A.; Maibach, H. I. Influence of age, anatomic site and race on skin roughness and scaliness. *Dermatology* **1998**, *196*, 401−407.

(42) Nazzaro-Porro, M.; Passi, S.; Boniforti, L.; Belsito, F. Effects of aging on fatty acids in skin surface lipids. *J. Invest. Dermatol.* **1979**, *73*, 112−117.

(43) Sun, X.; He, J.; Yang, X. Human breath as a source of VOCs in the built environment, Part I: A method for sampling and detection species. *Build. Environ.* **2017**, *125*, 565−573.

(44) Corsi, R. L.; Siegel, J.; Karamalegos, A.; Simon, H.; Morrison, G. C. Personal reactive clouds: Introducing the concept of near-head chemistry. *Atmos. Environ.* **2007**, *41*, 3161−3165.

(45) Kleindienst, T. E.; Lewandowski, M.; Offenberg, J. H.; Jaoui, M.; Edney, E. O. Ozone-isoprene reaction: Re-examination of the formation of secondary organic aerosol. *Geophys. Res. Lett.* **2007**, *34*, L01805.

(46) Liu, Q.; Abbatt, J. P. D. Liquid crystal display screens as a source for indoor volatile organic compounds. *Proc. Natl. Acad. Sci. U.S.A.* **2021**, *118*, No. e2105067118.

(47) Nicolaides, N. Skin lipids: Their biochemical uniqueness. *Science* **1974**, *186*, 19−26.

(48) Ehn, M.; Thornton, J. A.; Kleist, E.; Sipilä, M.; Junninen, H.; Pullinen, I.; Springer, M.; Rubach, F.; Tillmann, R.; Lee, B.; Lopez-Hilfiker, F.; Andres, S.; Acir, I.-H.; Rissanen, M.; Jokinen, T.; Schobesberger, S.; Kangasluoma, J.; Kontkanen, J.; Nieminen, T.; Kurtén, T.; Nielsen, L. B.; Jørgensen, S.; Kjaergaard, H. G.; Canagaratna, M.; Maso, M. D.; Berndt, T.; Petäjä, T.; Wahner, A.; Kerminen, V.-M.; Kulmala, M.; Worsnop, D. R.; Wildt, J.; Mentel, T. F. A large source of low-volatility secondary organic aerosol. *Nature* **2014**, *506*, 476−479.

(49) Kroll, J. H.; Seinfeld, J. H. Chemistry of secondary organic aerosol: Formation and evolution of low-volatility organics in the atmosphere. *Atmos. Environ.* **2008**, *42*, 3593−3624.

(50) Avery, A. M.; Waring, M. S.; DeCarlo, P. F. Human occupant contribution to secondary aerosol mass in the indoor environment. *Environ. Sci.: Processes Impacts* **2019**, *21*, 1301−1312.

(51) Lai, K.; Alvin, C.; Nazaroff; William, W. Modeling indoor particle deposition from turbulent flow onto smooth surfaces. *J. Aerosol Sci.* **2000**, *31*, 463−476.

(52) Docherty, K. S.; Wu, W.; Lim, Y. B.; Ziemann, P. J. Contributions of organic peroxides to secondary aerosol formed from reactions of monoterpenes with $O_3$. *Environ. Sci. Technol.* **2005**, *39*, 4049−4059.

(53) Nah, T.; Kessler, S. H.; Daumit, K. E.; Kroll, J. H.; Leone, S. R.; Wilson, K. R. Influence of molecular structure and chemical functionality on the heterogeneous OH-initiated oxidation of unsaturated organic particles. *J. Phys. Chem. A* **2014**, *118*, 4106−4119.

(54) Henze, D. K.; Seinfeld, J. H. Global secondary organic aerosol from isoprene oxidation. *Geophys. Res. Lett.* **2006**, *33*, L09812.

(55) Na, K.; Song, C.; Switzer, C.; Cocker, D. R. Effect of ammonia on secondary organic aerosol formation from α-pinene ozonolysis in dry and humid conditions. *Environ. Sci. Technol.* **2007**, *41*, 6096−6102.

(56) Hao, L.; Kari, E.; Leskinen, A.; Worsnop, D. R.; Virtanen, A. Direct contribution of ammonia to α-pinene secondary organic aerosol formation. *Atmos. Chem. Phys.* **2020**, *20*, 14393−14405.

(57) Nazaroff, W. W.; Weschler, C. J. Indoor acids and bases. *Indoor Air* **2020**, *30*, 559−644.

(58) Ortega, I. K.; Kupiainen, O.; Kurtén, T.; Olenius, T.; Wilkman, O.; McGrath, M. J.; Loukonen, V.; Vehkamäki, H. From quantum chemical formation free energies to evaporation rates. *Atmos. Chem. Phys.* **2012**, *12*, 225−235.

(59) Chen, H.; Varner, M. E.; Gerber, R. B.; Finlayson-Pitts, B. J. Reactions of methanesulfonic acid with amines and ammonia as a source of new particles in air. *J. Phys. Chem. B* **2016**, *120*, 1526−1536.

(60) Elm, J. Toward a holistic understanding of the formation and growth of atmospheric molecular clusters: A quantum machine learning perspective. *J. Phys. Chem. A* **2021**, *125*, 895−902.

(61) Praske, E.; Otkjær, R. v.; Crounse, J. D.; Hethcox, J. C.; Stoltz, B. M.; Kjaergaard, H. G.; Wennberg, P. O. Atmospheric autoxidation is increasingly important in urban and suburban North America. *Proc. Natl. Acad. Sci. U.S.A.* **2018**, *115*, 64−69.

(62) Pagonis, D.; Algrim, L. B.; Price, D. J.; Day, D. A.; Handschy, A. v.; Stark, H.; Miller, S. L.; de Gouw, J. A.; Jimenez, J. L.; Ziemann, P. J. Autoxidation of limonene emitted in a university art museum. *Environ. Sci. Technol. Lett.* **2019**, *6*, 520−524.

(63) Zeng, M.; Heine, N.; Wilson, K. R. Evidence that Criegee intermediates drive autoxidation in unsaturated lipids. *Proc. Natl. Acad. Sci. U.S.A.* **2020**, *117*, 4486−4490.

(64) Chan, T.; Cai, R.; Ahonen, L. R.; Liu, Y.; Zhou, Y.; Vanhanen, J.; Dada, L.; Chao, Y.; Liu, Y.; Wang, L.; Kulmala, M.; Kangasluoma, J. Assessment of Particle Size Magnifier inversion methods to obtain the particle size distribution from atmospheric measurements. *Atmos. Meas. Tech.* **2020**, *13*, 4885−4898.

(65) Wang, N.; Zannoni, N.; Ernle, L.; Bekö, G.; Wargocki, P.; Li, M.; Weschler, C. J.; Williams, J. Total OH reactivity of emissions from humans: in-situ measurement and budget analysis. *Environ. Sci. Technol.* **2021**, *55*, 149−159.

(66) Weschler, C. J.; Langer, S.; Fischer, A.; Bekö, G.; Toftum, J.; Clausen, G. Squalene and cholesterol in dust from Danish homes and daycare centers. *Environ. Sci. Technol.* **2011**, *45*, 3872−3879.

(67) Liu, Y.; Misztal, P. K.; Arata, C.; Weschler, C. J.; Nazaroff, W. W.; Goldstein, A. H. Observing ozone chemistry in an occupied residence. *Proc. Natl. Acad. Sci. U.S.A.* **2021**, *118*, No. e2018140118.

(68) Salonen, H.; Salthammer, T.; Morawska, L. Human exposure to ozone in school and office indoor environments. *Environ. Int.* **2018**, *119*, 503−514.

(69) Yang, S.; Zhu, Z.; Wei, F.; Yang, X. Carbon nanotubes/activated carbon fiber based air filter media for simultaneous removal of particulate matter and ozone. *Build. Environ.* **2017**, *125*, 60−66.

(70) Yang, S.; Nie, J.; Wei, F.; Yang, X. Removal of ozone by carbon nanotubes/quartz fiber film. *Environ. Sci. Technol.* **2016**, *50*, 9592−9598.

(71) Weschler, C. J. Ozone in indoor environments: concentration and chemistry. *Indoor Air* **2000**, *10*, 269−288.

(72) Nazaroff, W. W.; Weschler, C. J. Indoor ozone: Concentrations and implications. *Indoor Air* **2021**, DOI: 10.1111/ina.12942.